Scientific paper

Metal and Non-Metal Modified Titania: the Effect of Phase Composition and Surface Area on Photocatalytic Activity

Boštjan Žener,[1] Lev Matoh,[1] Martin Reli,[2] Andrijana Sever Škapin[3,4] and Romana Cerc Korošec[1,*]

[1] *Faculty of Chemistry and Chemical Technology, University of Ljubljana, Večna pot 113, 1000 Ljubljana, Slovenia;*

[2] *Institute of Environmental Technology, VŠB-Technical University of Ostrava, 17. listopadu 15/2172, Ostrava-Poruba, Czech Republic;*

[3] *Slovenian National Building and Civil Engineering Institute, Dimičeva 12, 1000 Ljubljana, Slovenia*

[4] *Faculty of Polymer Technology - FTPO, Ozare 19, 2380, Slovenj Gradec, Slovenia*

[*] *Corresponding author: E-mail: romana.cerc-korosec@fkkt.uni-lj.si*

Received: 10-11-2021

Abstract

The application of TiO_2 photocatalysis in various environmental fields has been extensively studied in the last decades due to its ability to induce the degradation of adsorbed organic pollutants. In the present work, TiO_2 powders doped and co-doped with sulfur and nitrogen and modified with platinum were prepared by particulate sol-gel synthesis. PXRD measurements revealed that the replacement of HCl with H_2SO_4 during synthesis reduced the size of the crystallites from ~ 30 nm to ~20 nm, increasing the surface area from ~44 m^2/g to ~80 m^2/g. This is consistent with the photocatalytic activity of the samples and the measured photocurrent behavior of the photocatalysts. The results showed that the properties of the powders (i.e., surface area, crystallite size, photocurrent behavior) depend strongly not only on the type but also on the amount of acid and dopants used in the synthesis. Doping, co-doping and modification of TiO_2 samples with nitrogen, sulfur and platinum increased their photocatalytic activity up to 6 times.

Keywords: Titanium dioxide; powders; doping; photocatalysis; photocurrent; SEM

1. Introduction

Titanium dioxide is considered to be one of the most contemporary important materials. It occurs in nature in three polymorphic modifications: anatase, rutile and brookite, among which rutile is the most abundant and thermodynamically stable. On the contrary, anatase has the highest photocatalytic activity, which can be attributed to the highest number of hydroxyl groups on the surface.[1] Furthermore, three metastable phases can be produced synthetically, one of which is β-TiO_2, which crystallizes in a monoclinic crystal system.[2,3] Due to its favourable properties, including its high chemical stability, non-toxicity, low price and high refractive index (value of μ is 2.70 for rutile and 2.55 for anatase) TiO_2 is used for a wide number of applications in a variety of fields, for example as a white pigment in paints, plastic, paper, toothpastes and chewing gums, replacing the toxic lead oxides.[4] It is also used in the fields of photovoltaics, electrochemistry and photocatalysis.[5–9]

Due to its ability to mineralize adsorbed organic pollutants to CO_2 and H_2O, photocatalysis has been researched extensively with regard to its application in the fields of water remediation and air purification.[10–12] Oxidation of adsorbed organic pollutants can occur directly on the surface of the photocatalyst.[13] In the case that adsorption is not favourable due to the same electric charge on both pollutant and catalyst itself, reactive hydroxyl radical, formed via oxidation of water with holes, can start degradation reactions of pollutants in a solution. To enhance photocatalytic efficiency, it is necessary to prevent recombination between holes and electrons on route to the surface or on the surface sites.[14]

Various studies have been aimed at increasing the photocatalytic activity of TiO_2, which can be achieved by increasing the surface area of TiO_2, or through metal and non-metal doping. The surface area of the photocatalyst can be increased by decreasing its particle size.[15,16] Samples with a smaller crystallite size have a larger number of surface active sites, which should also increase its photocatalytic activity. Wang *et al.,* however, concluded that an optimum particle size of 11 nm exists for the degradation of chloroform in water. This was attributed to an increased recombination rate, which offsets the ultra-high surface area.[17,18] Maira *et al.* found an optimum particle size of 7 nm for gas phase photooxidation of trichloroethylene. The diminished activity for samples with crystallites, smaller than 7 nm, was attributed to changes in electronic and structural properties.[19] The surface area of the photocatalyst can also be increased by adding polymers during the synthesis. The calcination that follows removes the polymer chains, leaving behind a mesoporous framework of TiO_2, with an increased surface area.[20–23]

Doping TiO_2 with metals also increases its photocatalytic activity, by facilitating free electron capture and thus extending the lifetime of photogenerated electron-hole pairs.[24] The capture results in an efficient separation of electron-hole pairs, thus inhibiting recombination and increasing the photocatalytic activity of TiO_2 by enhancing the mass transfer of holes and possibly electrons to the surface.[25] It has to be mentioned, however, that metal centres can also act as recombination centres and thus lower the photocatalytic activity. TiO_2 is usually doped with noble metals, such as Ag, Pt and Pd.[26–28] Other metals include Cu, V, Cr, Ni, as well as In.[29–31]

TiO_2 can be synthesized using various synthetic procedures, including hydrothermal, microwave-assisted and sonochemical methods, and miniemulsion techniques.[32–35] Sol-gel synthesis offers many benefits compared to the synthetic methods mentioned above, including low cost, simplicity and low preparation temperatures. Because of this, it is a well-established procedure for the preparation of metal oxide nanoparticles.[36] The method is based on initial hydrolysis of a precursor (e.g. $TiCl_4$, titanium alkoxides), which is followed by reactions of condensation (oxolation and olation). Reactions result in the formation of sols, which are defined as stable suspensions of colloidal particles that can polymerize to form gels under certain conditions. On the other hand, stable sol can be deposited by dip- or spin coating onto a substrate and is then subjected to a drying process. During this process, the free –OH groups begin to link together, resulting in xerogels.[37]

In this work, we focussed on the preparation and characterization of sulfur and nitrogen doped and co-doped and platinum modified TiO_2 powders. Synthesis, structural properties and photocatalytic efficiency of the corresponding thin film was already published.[38] Since chemically equivalent thin films and powders often behave in different way, we have also systematically studied powdered samples, which is the main focus of the presented paper. Different analytical methods were used for their characterization and determination of the photocatalytic activity. Prepared samples were characterized by X-ray diffraction (XRD), specific surface area (BET) and photocurrent measurements. Morphology of the powders was examined using a field emission scanning electron microscopy. The photocatalytic activity of the powders was determined by monitoring the rate of oxidation of isopropanol to acetone using FTIR spectroscopy.

2. Experimental

2. 1. Synthesis

The method of synthesis, as used to synthesize metal and non-metal doped and co-doped TiO_2 powders, has been described previously in detail elsewhere.[38] The synthesis procedure is described in the supplementary material.

Sample names, types and amounts of dopants and acids added during the synthesis are presented in Table 1.

Table 1. Sample names, types and amounts of dopants and acids added during the synthesis.

Sample	Dopant; dopant source	Nominal amount of dopant relative to TiO_2 (atom %)	Amount (mL) and type of acid added
REF	/	/	18; HCl
Urea_15	N; urea	15	18; HCl
Thiourea_15	S; Thiourea	15	18; HCl
S2	S; H_2SO_4	/	3.3; H_2SO_4
S3	S; H_2SO_4	/	4.95; H_2SO_4
S3_N0.5	S; H_2SO_4 N; NH_4NO_3	/ 0.5	4.95; H_2SO_4
S3_N2	S; H_2SO_4 N; NH_4NO_3	/ 2	4.95; H_2SO_4
S3_urea15	S; H_2SO_4 N; urea	/ 15	4.95; H_2SO_4
S3_thiourea15	S; H_2SO_4 S; Thiourea	/ 15	4.95; H_2SO_4
S3_N0.5+1%Pt	S; H_2SO_4 N; NH_4NO_3 Pt; H_2PtCl_6	/ 0.5 1	4.95; H_2SO_4
S3_N0.5+2%Pt	S; H_2SO_4 N; NH_4NO_3 Pt; H_2PtCl_6	/ 0.5 2	4.95; H_2SO_4
S3_N0.5+3%Pt	S; H_2SO_4 N; NH_4NO_3 Pt; H_2PtCl_6	/ 0.5 3	4.95; H_2SO_4
S3_urea15+1%Pt	S; H_2SO_4 N; urea Pt; H_2PtCl_6	/ 15 1	4.95; H_2SO_4
S3_urea15+2%Pt	S; H_2SO_4 N; urea Pt; H_2PtCl_6	/ 15 2	4.95; H_2SO_4

The measured amounts of different dopants were determined with XPS measurements and are given in.[38]

2. 2. Characterization

XRD patterns were measured using a PANalytical X'Pert PRO MPD instrument in the 2θ range of 20–80° with a step of 0.034° using CuKα1 radiation. The average diameters of crystallites and phase compositions (amounts of polymophic modifications in %) of the samples and corresponding error values were calculated with Rietveld analysis using TopasR software.[39] Structural model (ICSD codes 92363 for anatase and 171670 for β-TiO_2) was used for the calculations.

The specific surface area of the powders was determined through the measurement of nitrogen adsorption-desorption isotherms by a Tristar 3000, Micromeritics (USA) instrument. The measurements were performed at –196 °C (77 K). The samples were outgassed under vacuum for 16 h at 110 °C (383 K). The mass of the samples in the analyser was ≈ 0.1 g. The specific surface area was calculated from the adsorption measurements in the relative pressure ($p/p0$) range of 0.05–0.25.

Photocurrent responses were recorded using a three electrode system, where Ag/AgCl and a Pt wire were used as reference and counter electrodes, respectively. The working electrode was prepared by depositing the measured sample on the conductive side of an ITO foil. 0.1 M KNO_3 was used as an electrolyte. The measurements were carried out in the range of wavelengths from 250 nm to 450 nm at an applied external potential of 1 V. This ensures that the highest number of photogenerated electrons travel to the working electrode. In this way the charge carriers (free electrons and holes) were successfully separated, thus preventing recombination. Before each measurement, the cell was purged with argon in order to ensure an oxygen free environment.[40,41] In the measured range from 250 nm to 450 nm, the wavelength is being changed by 10 nm step. The photocurrent signal drops down when the shutter closes to switch the wavelength for another 10 nm.

The morphology and the size of the particles of prepared powders were examined using a field-emission scanning electron microscope FE-SEM (FEI Inspect^{TM} F50 and Ultra Plus Zeiss). Accelerating voltage was set to 2 kV. Images were obtained with detection of secondary electrons.

2. 3. Photocatalytic Activity Tests

The photocatalytic activity of the powder samples under UV and visible light exposure was determined by measuring the rate constant of oxidation of isopropanol to acetone and further oxidation leading to CO_2 and H_2O as the final products using FTIR spectroscopy. Commercially available Hombikat UV 100 (DE) – anatase nanopowder, with a primary crystal size <10 nm and specific surface area >250 m^2/g was used for comparison. The reactions are presented in Equation (2):[42]

$$isopropanol \overset{k_0}{\rightarrow} acetone \overset{k_1}{\rightarrow} further\ oxidation\ products \quad (2)$$

Generally, the first step (k_0) is considered to be a zero order reaction, whereas the second step (k_1) is considered to be first order reaction. The method is presented in detail elsewhere.[43] In the first step, approximately 50 mg of the powder was suspended in 3 mL of 1-butanol. This suspension was then evenly distributed in a standard Petri dish and dried for 2 hours at 50 °C. Each dried sample was then put in a sealed gas-solid flow reactor system and then injected with 8 μL of isopropanol. Once the adsorption equilibrium was reached, as indicated by flat line in the isopropanol concentration profile, the sample was illuminated with a 300 W Xe lamp (Newport Oriel Instrument) with an infrared filter. The spectrum of this Xe lamp is similar to sun illumination. The working distance between the Petri dish and the lamp was 6 cm. The temperature and relative humidity were set to 23 ± 2 °C and 25 ± 5 %, respectively. The isopropanol degradation and acetone formation and degradation processes (see equation 2) were followed by monitoring the calculated area of their characteristic peaks at 951 cm^{-1} and 1207 cm^{-1}, respectively, in the IR spectra obtained by a FT-IR spectrometer (Perkin-Elmer Spectrum BX II). The examples of characteristic FTIR output at three diferent reaction times with related explanations are presented in Figure S1 (Supplementary material).

3. Results and Discussion

3. 1. X-Ray diffraction (XRD)

XRD patterns of the prepared powders are presented in Figure 1. It can be seen from the results that anatase is the only polymorphic modification present in samples synthesized with HCl (REF, Urea_15 and Thiourea_15). On the contrary, patterns of samples synthesized with H_2SO_4 include peaks of β-TiO_2, which crystallizes in a monoclinic crystal system and cannot be found in nature. Table 2 shows the share of polymorphic phases and calculated diameters of crystallites (both were calculated using the *Rietveld analysis*) in characterized samples. The results show that the amount of β-TiO_2 in samples synthesized with H_2SO_4 varies from 15.6 ± 0.3 % to 45.4 ± 0.3 %. The highest amounts are present in samples S3_urea15 and S3_thiourea15 (38.7 ± 0.3 % and 45.4 ± 0.3 %), whereas samples S3 exhibits the lowest (15.6 ± 0.3 %). Moreover, crystallites found in samples synthesized with H_2SO_4 (15.1 ± 0.3 – 23.5 ± 0.2 nm) were smaller compared to samples synthesized with HCl (26.9 ± 0.7 – 30.7 ± 0.8 nm). The same trend was observed in our previously published work, which focused on thin films.[38] As with thin film sys-

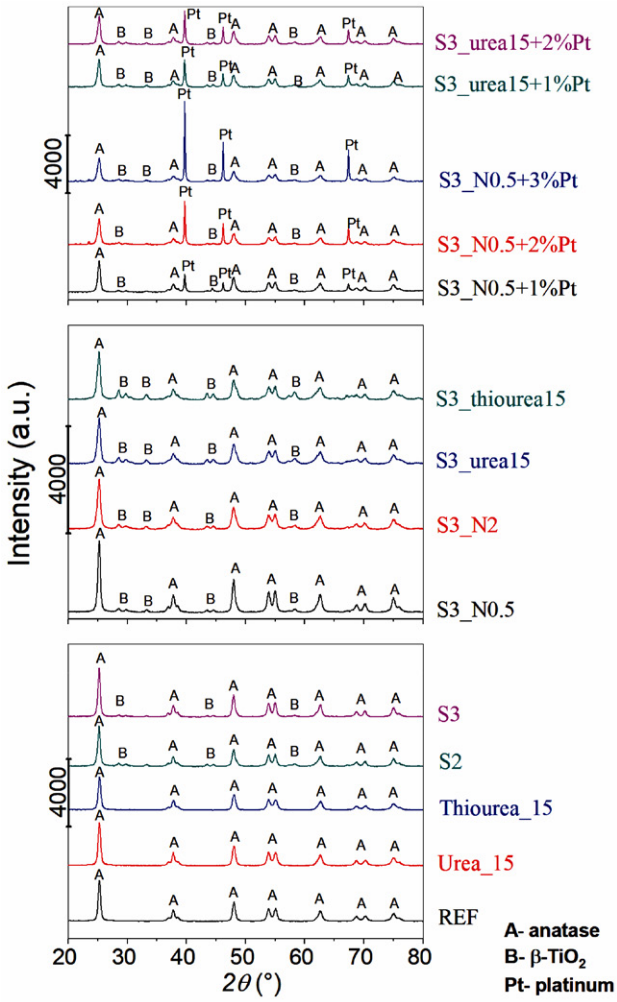

Figure 1. X-Ray diffraction patterns of powders. The designations A, B and Pt indicate the peaks for the corresponding TiO_2 polymorphic modifications and platinum.

tems, this can be attributed to the formation of $TiOSO_4$ in samples synthesized with H_2SO_4, which inhibits the crystallization of anatase. The smallest crystallites were found in samples S3_N2 and S3_urea15 (15.1 ± 0.3 to 17.5 ± 0.2 nm). Decreasing the crystallite size of TiO_2 usually results in an increase in surface area, which can have a positive effect on the photocatalytic activity of the samples. In most samples, the calculated crystallite sizes of β-TiO_2 are smaller to those of anatase.

When comparing the size of crystallites in powders to those in thin films (as published in our previous work), we observed an interesting phenomenon. In the case of samples synthesized with H_2SO_4 we found larger crystallites in powder form (sizes of ~ 15 – 23 nm in powders compared to 8–12 nm in thin films). This can be explained by the unlimited growth of crystallites in powders, unlike in thin films, where growth is limited by the thickness of the film and the substrate. In direct contrast, when analysing samples synthesized with HCl we found larger crystallites in thin film samples compared to powders (sizes of 40 – 60 nm and ~ 27 – 31 nm, respectively). We attribute this to the partial crystallization and subsequent growth of TiO_2 nanoparticles during the thermal treatment after each deposition (the final layer was prepared from three successive depositions, after each deposition thermal treatment was performed at 300 °C).[38]

Samples with added platinum also exhibit peaks at 40, 47.5 and 67.5° *2θ*, which correspond to metallic platinum.

3. 2. Specific Surface Area (BET)

Results of surface area measurements are presented in Table 2. Measurements for six of these samples (REF, Urea_15, Thiourea_15, S3, S3_N0.5 and S3_N0.5+1% Pt)

Table 2. The share of different polymorphic modifications, sizes of crystallites in powder samples calculated from XRD patterns using Rietveld refinement and the specific surface areas for examined samples.

Sample	Amount of anatase (wt%)	Calculated diameters of anatase crystallites (nm)	Amount of β-TiO_2 (wt%)	Calculated diameters of β-TiO_2 crystallites (nm)	BET specific surface area (m^2/g)
REF	100	30.7 ± 0.8	/	/	44.1 ± 0.4
Urea_15	100	29.6 ± 0.7	/	/	24.2 ± 0.2
Thiourea_15	100	26.9 ± 0.7	/	/	49.5 ± 0.3
S2	75.1 ± 0.3	21.1 ± 0.1	24.9 ± 0.3	19.0 ± 0.5	63.2 ± 0.3
S3	84.4 ± 0.3	23.5 ± 0.2	15.6 ± 0.3	19.0 ± 0.7	80.2 ± 0.2
S3_N0.5	81.1 ± 0.4	22.3 ± 0.2	18.9 ± 0.4	18.8 ± 0.6	84.5 ± 0.3
S3_N2	69.9 ± 0.3	16.8 ± 0.1	30.1 ± 0.3	15.1 ± 0.3	103.4 ± 0.4
S3_urea15	61.3 ± 0.3	17.5 ± 0.2	38.7 ± 0.3	16.5 ± 0.3	101.7 ± 0.4
S3_thiourea15	54.6 ± 0.3	18.7 ± 0.2	45.4 ± 0.3	19.3 ± 0.3	92.1 ± 0.3
S3_N0.5+1%Pt	82 ± 1	21.0 ± 0.4	18 ± 1	18 ± 1	83.7 ± 0.2
S3_N0.5+2%Pt	77 ± 2	17.9 ± 0.6	23 ± 2	20 ± 3	80.5 ± 0.4
S3_N0.5+3%Pt	74 ± 2	17.1 ± 0.8	26 ± 2	20 ± 3	84.1 ± 0.4
S3_urea15+1%Pt	69 ± 1	21.0 ± 0.6	31 ± 1	22 ± 2	82.3 ± 0.3
S3_urea15+2%Pt	73 ± 1	20.7 ± 0.6	27 ± 1	23 ± 2	84.2 ± 0.4

have already been published in our previous article. This study expands on those results.[38]

In general, samples synthesized with H_2SO_4 have higher surface areas (63.2 ± 0.3 to 103.4 ± 0.4 m^2/g) compared to samples synthesized with HCl (24.2 ± 0.2 to 49.5 ± 0.3 m^2/g). The higher surface area can be attributed to smaller crystallites found in samples synthesized with the addition of H_2SO_4, which is also observed from the XRD measurements.

It can be seen from the results presented in Table 2 that the addition of urea (sample Urea_15 has specific surface area of 24.2 ± 0.2 m^2/g) significantly decreases the surface area compared to the undoped sample REF (44.1 ± 0.4 m^2/g). By increasing the volume of H_2SO_4 added we also increase the surface area of the sample (63.2 ± 0.3 m^2/g for S2, 80.2 ± 0.2 m^2/g for S3). The addition of NH_4NO_3 (samples S3_N0.5 and S3_N2), urea (sample S3_urea15) and thiourea (sample S3_thiourea15) to sample S3 also increase the surface area of the samples (surface areas 84.5 ± 0.3 to 103.4 ± 0.4 m^2/g). This can be explained by an additional decrease in the size of crystallites in these samples as compared to those in sample S3.

The specific surface area does not change significantly when adding 1 % and 3 % of Pt to sample S3_N0.5. On the contrary, a decrease in surface area is observed when adding 2 % of Pt to sample S3_N0.5 (from 84.5 ± 0.3 m^2/g for sample S3_N0.5 to 80.5 ± 0.4 m^2/g for sample S3_N0.5+2%Pt) and when adding 1 % or 2 % of Pt to sample S3_urea15 (from 101.7 ± 0.4 m^2/g for S3_urea15 to 82.3 ± 0.3 m^2/g and 84.2 ± 0.4 m^2/g for sample S3_urea15+1%Pt and S3_urea15 + 2%Pt, respectively).

3. 3. Scanning Electron Microscopy (SEM)

Figure 2 shows FE-SEM micrographs of samples REF, S3_N0.5 and S3_thiourea15. Substituting HCl (sample REF) with H_2SO_4 (samples S3_N0.5 and S3_thiourea15) during the synthesis has resulted in the formation of more porous powders, which is in agreement with the results of BET specific surface area measurements. Furthermore, we have observed crystallites of sizes 31–35 nm in the SEM image of sample REF, which confirms the results of the XRD measurements. SEM images of samples synthesized with H_2SO_4 show crystallites ranging in size from 20–22 nm (sample S3_N0.5) and 18–23 nm (sample S3_thiourea15), which is also in agreement with the results of XRD measurements. We can also observe pores with sizes ranging from 70-100 nm (sample S3_N0.5) and 70-80 nm (sample S3_thiourea15).

3. 4. Photocurrent Measurements

Figure 3 shows the results of photocurrent measurements for different samples. The reason why there is a very low photocurrent response in UV region is due to the fact 150 W Xe lamp was used as the light source. Xe lamps have very low intensity in UV region below 300 nm.

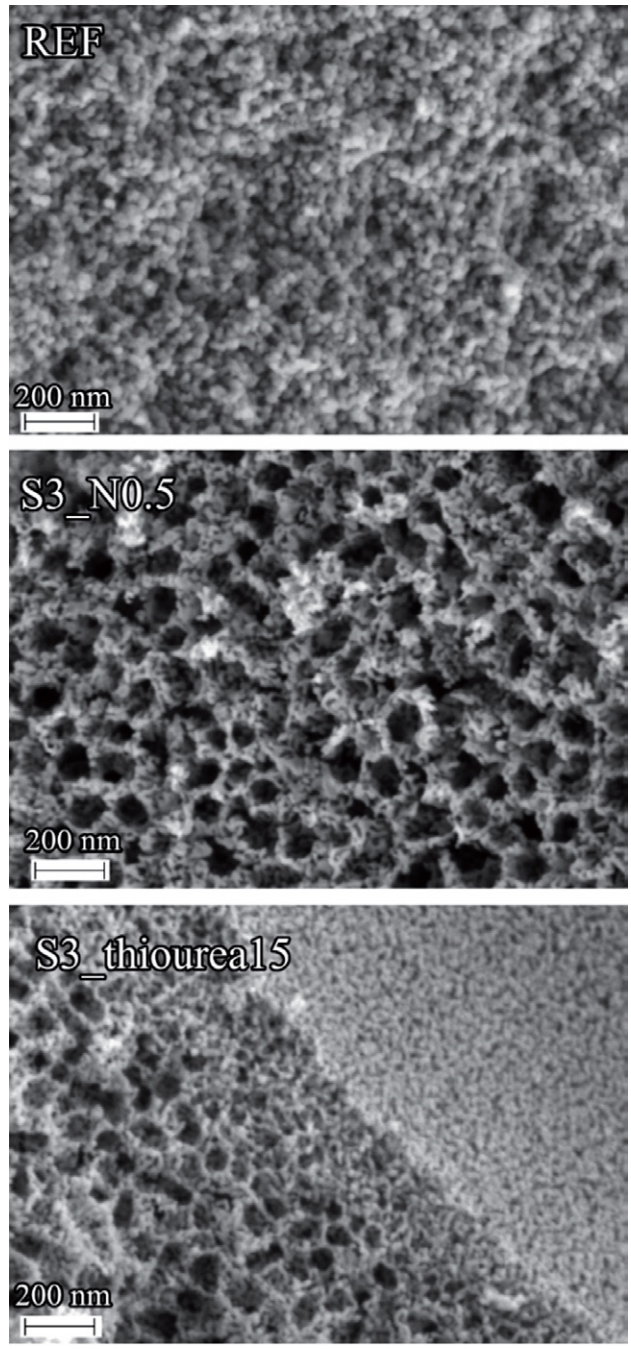

Figure 2. FE-SEM micrographs of powders: REF, S3_N0.5 and S3_thiourea15 at 200,000x magnification. Accelerating voltage was set to 2 kV. Images were obtained with detection of secondary electrons.

By adding urea (sample Urea_15) to the undoped sample REF, the photocurrent response has decreased. We can attribute this to the lower surface area of sample Urea_15, which was observed from BET measurements. Contrarily, the addition of thiourea (sample Thiourea_15) has resulted in an increase in photocurrent response, which is attributed to the higher surface area of the sample Thiourea_15.

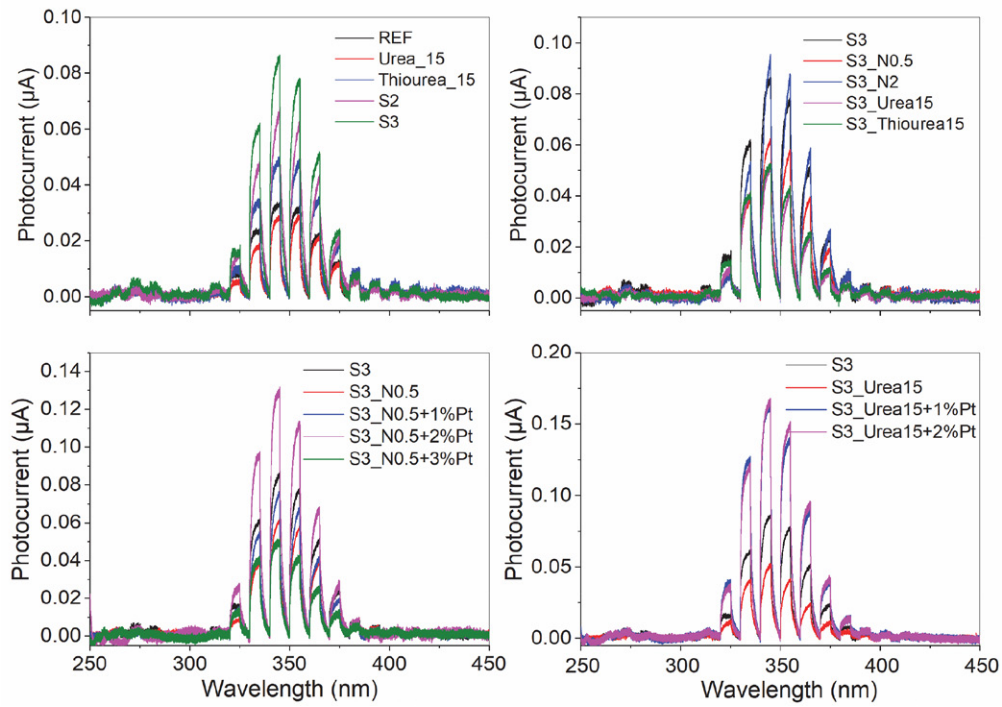

Figure 3. Photocurrent responses recorded under applied external potential of 1 V.

By substituting HCl with H_2SO_4 during the synthesis (samples S2 and S3) the current has increased. As with sample Thiourea_15, this can be explained by the higher surface area of samples S2 and S3 compared to the samples synthesized with HCl. Because sample S3 has a higher surface area than sample S2, a higher photocurrent is induced when irradiating the former. The results, as presented in Figure 3b, show that the addition of 0.5 % of NH_4NO_3 (sample S3_N0.5), urea (sample S3_urea15) or thiourea (sample S3_thiourea15) to sample S3 has resulted in a decrease in photocurrent response, despite the increase in surface area. The response has increased when adding 2 % of NH_4NO_3 (sample S3_N2), which also has the highest surface area of all the samples. From this we can deduce that the amount of induced photocurrent depends not only on the surface area, but also on the amount of added dopants. Band gap energies for selected samples have already been measured and published by Žener et al. [38]

Results for samples with added Pt are presented in Figures 3c and 3d. When comparing these samples with those without the added Pt (samples S3_N0.5 and S3_urea15), we can see that the addition of 1 % and 2 % of Pt had a positive effect on the photocatalytic response, despite the lower surface area of these samples. When irradiating the sample with 3 % of added Pt (sample S3_N0.5 + 3%Pt) the amount of induced photocurrent has decreased dramatically, which could be due to the increased Pt blocking light to the photocatalyst. Moreover, platinum particles can also act as recombination centres.

3. 5. Photocatalytic Activity

Concentration profiles for isopropanol and acetone for selected samples are presented in Figure 4. The photocatalytic activity of powders under UV and visible light irradiation was tested by monitoring the oxidation of isopropanol to acetone. It can be seen that the isopropanol curve is unstable before the UV and visible light is switched on, which can be attributed to the adsorption of isopropanol onto the surface of the sample and reactor system. After the UV and visible light is switched on the acetone concentration increases, while the isopropanol concentration decreases. Reactions are presented in Equation (2) in the experimental section. In the initial steps of the photocatalysis, we can approximate the reaction to be of zero order, because the photocatalytic oxidation of isopropanol to acetone is faster than the subsequent oxidation of acetone. Zero order kinetics can be described with Equation (3):

$$c = k_0 t + c_0 \quad (3)$$

In this equation c and c_0 represent concentration of acetone and the initial concentration of acetone, respectively in ppm, while t is time in hours and k_0 is the zero-order rate constant (units ppm/h). Therefore, the initial slope of the acetone concentration curve is equal to k_0 (Equation (3)), which was determined from line equations in Figure 4. This presents a good basis to compare photocatalytic activity of different TiO_2 powders.[43] Zero order rate constants (k_0) for different samples are presented in Table 3.

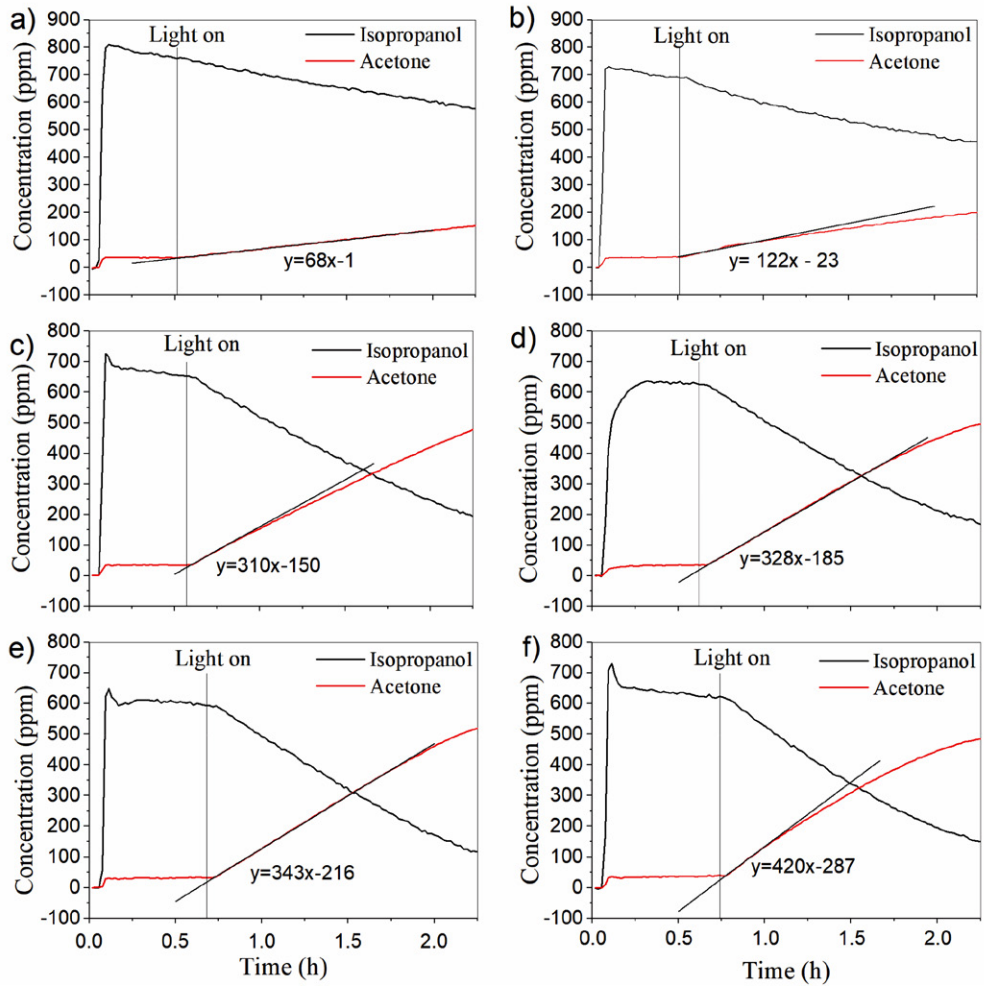

Figure 4. Concentration profiles of isopropanol and acetone for: (a) REF; (b) Urea_15; (c) S3; (d) S3_N2; (e) S3_N0.5 + 1%Pt and (f) S3_urea15 + 1%Pt; y in the line equation represents concentration of acetone (in ppm) and x represents time of experiment in reactor (in hours)

Table 3. Photocatalytic activities of different samples, determined by observing the oxidation of isopropanol to acetone (rate constant k_0).

Sample	Activity under UV and visible light exposure - k_0 (ppm/h)
HOMBIKAT UV 100	337 ± 2
REF	68 ± 1
Urea_15	122 ± 4
Thiourea_15	50 ± 2
S2	183 ± 2
S3	310 ± 3
S3_N0.5	260 ± 2
S3_N2	328 ± 3
S3_urea15	304 ± 2
S3_thiourea15	225 ± 2
S3_N0.5+1%Pt	343 ± 2
S3_N0.5+2%Pt	251 ± 3
S3_N0.5+3%Pt	260 ± 3
S3_urea15+1%Pt	420 ± 3
S3_urea15+2%Pt	420 ± 2

The addition of urea (sample Urea_15) to the undoped sample REF has resulted in an increase in the photocatalytic activity (k_0 = 122 ± 4 ppm/h and 68 ± 1 ppm/h for sample Urea_15 and REF, respectively). In our previously published work, we reported a very high band-gap value in sample REF (3.44 eV). The addition of urea narrows the band-gap due to nitrogen doping, and consequently increases photocatalytic activity even under UV light.[38,44] On the contrary, addition of thiourea (sample Thiourea_15) decreases the photocatalytic activity of the sample (k_0 = 50 ± 2 ppm/h) when compared to REF, despite the former having a higher surface area (49.5 ± 0.3 m^2/g for sample Thiourea_15 and 44.1 ± 0.4 m^2/g for REF) and higher photocurrent response. This could be explained by higher recombination rates of the charge carriers in sample Thiourea_15. Additional measurements would, however, be needed to confirm this theory.

By using H_2SO_4 instead of HCl in the synthesis (samples S2 and S3) we obtained samples with smaller-sized crystallites, which results in higher porosity (24.2 ± 0.2 to 49.5 ± 0.3 m^2/g for samples synthesized with HCl; 63.2 ± 0.3

and 80.2 ± 0.2 m^2/g for samples S2 and S3, respectively) and a far higher photocurrent response. For these reasons, samples S2 and S3 show much higher activity than samples synthesized with HCl (k_0 = 183 ± 2 ppm/h for sample S2 and 310 ± 3 ppm/h for sample S3). S3 has a higher surface area and higher photocurrent response compared to S2, and consequently much higher photocatalytic activity.

The addition of NH_4NO_3 (samples S3_N0.5 and S3_N2), urea (sample S3_urea15) and thiourea (sample S3_thiourea_15) to sample S3 increases the specific surface areas (84.5 ± 0.3 to 103.4 ± 0.4 m^2/g). Despite this, only one sample has a higher photocatalytic activity than the sample without additions (sample S3, k_0 = 310 ± 3 ppm/h, sample S3_N2, k_0 = 328 /h). This can be explained by the results of the photocurrent measurements, which have shown decreased responses (compared to sample S3) in all but sample S3_N2, which also has the highest surface area (103.4 ± 0.4 m^2/g). Higher activity can also be attributed to the addition of nitrogen, which increases the amount of oxygen vacancies and reduces the band gap energy, resulting in higher photocatalytic activity.[38] The decreased activity in samples S3_urea15 and S3_thiourea15 can be attributed to higher percentages of β-TiO_2, found in these two samples, since the photocatalytic activity of β-TiO_2 is generally much lower than that of anatase.[45–47]

The addition of Pt to sample S3_N0.5 does not increase its surface area, in fact in the case of the sample with 2 % Pt added (sample S3_N0.5 + 2% Pt) it actually decreases (84.5 ± 0.3 m^2/g for sample S3_N0.5 and 80.5 ± 0.4 m^2/g for sample S3_N0.5 + 2% Pt). Despite this, the sample S3_N0.5 + 1%Pt shows much higher photocatalytic activity (k_0 = 343 ± 2 ppm/h), compared to sample S3_N0.5 (k_0 = 260 ± 2 ppm/h). We attribute this to Pt acting as an efficient trap for free electrons, thus inhibiting recombination (confirmed with photocurrent measurements), whilst also improving the free electron transfer to adsorbed pollutants. The activity of sample S3_N0.5+3%Pt is equal to the activity of sample S3_N0.5, but the activity of sample S3_N0.5 + 2%Pt has reduced slightly.

Doping the sample S3_urea15 with Pt (samples S3_urea15 + 1%Pt and S3_urea15+2%Pt) significantly lowers its surface area (82.3 ± 0.3 m^2/g for sample S3_urea15 + 1%Pt and 84.2 ± 0.4 m^2/g for sample S3_urea15 + 2%Pt). Furthermore, results of the photocurrent measurements have shown that the addition of Pt significantly increases the photocurrent response, resulting in far higher photocatalytic activity in samples S3_urea15 + 1%Pt (k_0 = 420 ± 3 ppm/h) and S3_urea15 + 2%Pt (k_0 = 420 ± 2 ppm/h) compared to sample S3_urea15 (k_0 = 304 ± 2 ppm/h). It was found out that metal and non-metal doping, as well as addition of HPC significantly increase the photocatalytic activity of powders under UV and visible light irradiation. In the case of samples S3_urea15 + 1%Pt and S3_urea15 + 2%Pt the photocatalytic activity is even higher than that of selected anatase sample available on the market: HOMBIKAT UV 100 (k_0 = 337 ± 2 ppm/h) (see Table 3).[48]

4. Conclusions

In the present work TiO_2 powders, doped with sulfur and nitrogen and modified with platinum were prepared by means of particulate sol-gel synthesis in order to increase the photocatalytic activity of undoped sample, while the organic polymer hydroxypropyl cellulose (HPC) was added to increase the surface area of the photocatalyst. By substituting HCl with H_2SO_4 during the synthesis, the resulting samples contained smaller crystallites (26.9 ± 0.7 – 30.7 ± 0.8 nm for samples synthesized with HCl; 15.1 ± 0.3 – 23.5 ± 0.2 nm nm for samples synthesized with H_2SO_4). We attributed the smaller crystallite size to the formation of $TiOSO_4$, which inhibits the crystallization of TiO_2. Additionally, we observed the presence of β-TiO_2 in samples synthesized with H_2SO_4. The highest percentage of β-TiO_2 was found in sample S3_thiourea15 (45.4 ± 0.3 %). The afore-mentioned decrease in the size of crystallites led to a higher specific surface area for samples synthesized with H_2SO_4 (63.2 ± 0.3 to 103.4 ± 0.4 m^2/g) compared to those synthesized with HCl (24.2 ± 0.2 to 49.5 ± 0.3 m^2/g). The addition of NH_4NO_3, urea and thiourea to sample S3 increased its porosity. Sample S3_N2 had the highest surface area (103.4 ± 0.4 m^2/g) and the smallest crystallites of anatase (16.8 ± 0.1 nm). The addition of Pt did not increase the sample's porosity, in some cases it even decreased it. FE-SEM images confirmed the increased porosity of samples synthesized with H_2SO_4. Additionally, smaller crystallites were found in samples synthesized with H_2SO_4, confirming the results of X-Ray diffraction.

The increased porosity of the samples synthesized with H_2SO_4 also resulted in greater photocurrent responses in these samples compared to those synthesized with HCl. Despite increasing the specific surface area, the addition of NH_4NO_3, urea and thiourea to S3 yielded a lower photocurrent response, with the exception of sample S3_N2, which also had the highest surface area. In all but one case the addition of platinum resulted in greater photocurrent responses.

Samples synthesized with H_2SO_4 exhibit higher photocatalytic activity compared to samples synthesized with HCl, which can be explained by larger surface areas and higher photocurrent responses. Out of all the samples with added NH_4NO_3, urea or thiourea, only sample S3_N2 has a higher photocatalytic activity compared to sample S3. This is also the only sample in this group which exhibit a greater photocurrent response than sample S3. The addition of platinum to sample S3_urea significantly increased its photocatalytic activity, which is in agreement with the results of photocurrent measurements. Out of all the samples, samples S3_urea15 + 1%Pt and S3_urea15 + 2%Pt showed the highest photocatalytic activity (k_0 = 420 ± 3 and 420 ± 2 ppm/h), which was even higher than the activity of the well-known pure anatase photocatalyst HOMBIKAT UV 100 (k_0 = 337 ± 2 ppm/h). We were able to significantly increase the photocatalytic activity of pow-

ders under UV and visible light irradiation by increasing the surface area and photocurrent response with non-metal and metal doping.

Acknowledgements

The authors acknowledge the financial support from the Slovenian Research Agency (research core funding Nos. P1-0134 and P2-0273, while part of the work was conducted under project No. NC-0002). B. Ž. is grateful to Slovenian Research Agency for the position of young researcher enabling him the doctoral study. M. R. also acknowledges the Operational Programme Research, Development and Education, project No. CZ.02.1.01./0.0/0.0/17 _049/0008419 „COOPERATION". The authors thank to Mojca Opresnik from the National Institute of Chemistry for BET measurements and to Edi Kranjc (also from the National Institute of Chemistry) for performing XRD measurements. The authors also acknowledge dr. Amalija Golobič for her help with Rietveld analysis.

5. References

1. R. Fagan, D. E. McCormack, D. D. Dionysiou, S. C. Pillai, *Mater. Sci. Semicond. Process.* **2016**, *42*, 2–14. **DOI:**10.1016/j.mssp.2015.07.052
2. R. Marchant, L. Brohan, M. Tournox, *Mater. Res. Bull.* **1980**, *15*, 1129–1133. **DOI:**10.1016/0025-5408(80)90076-8
3. S. León-Ríos, R. Espinoza González, S. Fuentes, E. Chávez Ángel, A. Echeverría, A. E. Serrano, C. S. Demergasso, R. A. Zárate, *J. Nanomater.* **2016**, *2016*, 1–8. **DOI:**10.1155/2016/7213672
4. T. Fröschl, U. Hörmann, P. Kubiak, G. Kučerová, M. Pfanzelt, C. K. Weiss, R. J. Behm, N. Hüsing, U. Kaiser, K. Landfester, M. Wohlfahrt-Mehrens, *Chem. Soc. Rev.* **2012**, *41*, 5313–5360. **DOI:**10.1039/c2cs35013k
5. M. Grätzel, *J. Sol- Gel Sci. Technol.* **2001**, *22*, 7–13. **DOI:**10.1023/A:1011273700573
6. M. Fitra, I. Daut, M. Irwanto, N. Gomesh, Y. M. Irwan, *Energy Procedia* **2013**, *36*, 278–286. **DOI:**10.1016/j.egypro.2013.07.032
7. M. Hassan, Y. Zhao, B. Xie, *Chem. Eng. J.* **2016**, *285*, 264–275. **DOI:**10.1016/j.cej.2015.09.093
8. M. Rozman, J. Cerar, M. Lukšič, M. Uršič, A. Mourtzikou, H. Spreizer, I. K. Škofic, E. Stathatos, *Electrochim. Acta* **2017**, *238*, 278–287. **DOI:**10.1016/j.electacta.2017.04.030
9. N. Amira Marfur, N. Farhana Jaafar, M. Khairuddean, N. Nordin, *Acta Chim. Slov.* **2020**, *67*, 361–374. **DOI:**10.17344/acsi.2019.5161
10. J.-M. Herrmann, C. Guillard, P. Pichat, *Catal. Today* **1993**, *17*, 7–20. **DOI:**10.1016/0920-5861(93)80003-J
11. H. Zhao, S. Chen, X. Quan, H. Yu, H. Zhao, *Appl. Catal. B Environ.* **2016**, *194*, 134–140. **DOI:**10.1016/j.apcatb.2016.04.042
12. J. Yu, P. Zhang, H. Yu, C. Trapalis, *Int. J. Photoenergy* **2012**, *2012*, 1–4. **DOI:**10.1155/2012/594214
13. Z. Xing, J. Zhang, J. Cui, J. Yin, T. Zhao, J. Kuang, Z. Xiu, N. Wan, W. Zhou, *Appl. Catal. B Environ.* **2018**, *225*, 452–467. **DOI:**10.1016/j.apcatb.2017.12.005
14. S. Zhu, D. Wang, *Adv. Energy Mater.* **2017**, *7*, 1–24. **DOI:**10.1002/aenm.201700841
15. C. B. Almquist, P. Biswas, *J. Catal.* **2002**, *212*, 145–156. **DOI:**10.1006/jcat.2002.3783
16. A. V. Vorontsov, E. N. Kabachkov, I. L. Balikhin, E. N. Kurkin, V. N. Troitskii, P. G. Smirniotis, *J. Adv. Oxid. Technol.* **2018**, *21*, 127–137. **DOI:**10.26802/jaots.2017.0063
17. C. C. Wang, Z. Zhang, J. Y. Ying, *Nanostructured Mater.* **1997**, *9*, 583–586. **DOI:**10.1016/S0965-9773(97)00130-X
18. Z. Zhang, C.-C. Wang, R. Zakaria, J. Y. Ying, *J. Phys. Chem. B* **2002**, *102*, 10871–10878. **DOI:**10.1021/jp982948+
19. A. J. Maira, K. L. Yeung, C. Y. Lee, P. L. Yue, C. K. Chan, *J. Catal.* **2000**, *192*, 185–196. **DOI:**10.1006/jcat.2000.2838
20. Y. Li, B. P. Bastakoti, M. Imura, S. M. Hwang, Z. Sun, J. H. Kim, S. X. Dou, Y. Yamauchi, *Chem. - A Eur. J.* **2014**, *20*, 6027–6032. **DOI:**10.1097/01.ccm.0000457553.95006.19
21. W. Dong, Y. Sun, C. W. Lee, W. Hua, X. Lu, Y. Shi, S. Zhang, J. Chen, D. Zhao, *J. Am. Chem. Soc.* **2007**, *129*, 13894–13904. **DOI:**10.1021/ja073804o
22. K. Kato, A. Tsuzuki, Y. Torii, H. Taoda, T. Kato, Y. Butsugan, *J. Mater. Sci.* **1995**, *30*, 837–841. **DOI:**10.1007/BF00356349
23. J. Zhang, Y. Deng, D. Gu, S. Wang, L. She, R. Che, Z. S. Wang, B. Tu, S. Xie, D. Zhao, *Adv. Energy Mater.* **2011**, *1*, 241–248. **DOI:**10.1002/aenm.201000004
24. J. Vargas Hernández, S. Coste, A. García Murillo, F. Carrillo Romo, A. Kassiba, *J. Alloys Compd.* **2017**, *710*, 355–363. **DOI:**10.1016/j.jallcom.2017.03.275
25. N. A. M. Barakat, M. A. Kanjwal, I. S. Chronakis, H. Y. Kim, *J. Mol. Catal. A Chem.* **2013**, *366*, 333–340. **DOI:**10.1016/j.molcata.2012.10.012
26. N. Sobana, M. Muruganadham, M. Swaminathan, *J. Mol. Catal. A Chem.* **2006**, *258*, 124–132. **DOI:**10.1016/j.molcata.2006.05.013
27. D. Hufschmidt, D. Bahnemann, J. J. Testa, C. A. Emilio, M. I. Litter, *J. Photochem. Photobiol. A Chem.* **2002**, *148*, 223–231. **DOI:**10.1016/S1010-6030(02)00048-5
28. S. Sakthivel, M. V. Shankar, M. Palanichamy, B. Arabindoo, D. W. Bahnemann, V. Murugesan, *Water Res.* **2004**, *38*, 3001–3008. **DOI:**10.1016/j.watres.2004.04.046
29. J. H. Kim, G. Kwon, H. Lim, C. Zhu, H. You, Y. T. Kim, *J. Power Sources* **2016**, *320*, 188–195. **DOI:**10.1016/j.jpowsour.2016.04.019
30. M. Tahir, N. A. S. Amin, *Appl. Catal. B Environ.* **2015**, *162*, 98–109. **DOI:**10.1016/j.apcatb.2014.06.037
31. R. Pol, M. Guerrero, E. García-Lecina, A. Altube, E. Rossinyol, S. Garroni, M. D. Baró, J. Pons, J. Sort, E. Pellicer, *Appl. Catal. B Environ.* **2016**, *181*, 270–278. **DOI:**10.1016/j.apcatb.2015.08.006
32. P. D. Cozzoli, A. Kornowski, H. Weller, *J. Am. Chem. Soc.* **2003**, *125*, 14539–14548. **DOI:**10.1021/ja036505h
33. X. Jia, W. He, X. Zhang, H. Zhao, Z. Li, Y. Feng, *Nanotechnology* **2007**, *18*, 075602. **DOI:**10.1088/0957-4484/18/7/075602

34. H. Xu, B. W. Zeiger, K. S. Suslick, *Chem. Soc. Rev.* **2013**, *42*, 2555–2567. **DOI:**10.1039/C2CS35282F
35. R. Rossmanith, C. K. Weiss, J. Geserick, N. Hüsing, U. Hörmann, U. Kaiser, K. Landfester, *Chem. Mater.* **2008**, *20*, 5768–5780. **DOI:**10.1021/cm800533a
36. B. G. Rao, D. Mukherjee, B. M. Reddy, in *Nanostructures Nov. Ther. Synth. Charact. Appl.* (Eds.: D. Ficai, A.M. Grumezescu), Elsevier Inc., Oxford, **2017**, pp. 1–31.
37. U. Schubert, N. Hüsing, *Synthesis of Inorganic Materials*, Wiley-VCH Verlag, Weinheim, **2012**.
38. B. Žener, L. Matoh, G. Carraro, B. Miljević, R. Cerc Korošec, *Beilstein J. Nanotechnol.* **2018**, *9*, 1629–1640. **DOI:**10.3762/bjnano.9.155
39. General Profile and Structure Analysis Software for Powder Diffraction Data, Topas version 2.1, Bruker AXS, Karlsruhe, Germany, **2000**.
40. M. Reli, I. Troppová, M. Šihor, J. Pavlovský, P. Praus, K. Kočí, *Appl. Surf. Sci.* **2019**, *469*, 181–191. **DOI:**10.1016/j.apsusc.2018.10.255
41. M. Reli, P. Huo, M. Šihor, N. Ambrožová, I. Troppová, L. Matějová, J. Lang, L. Svoboda, P. Kuśtrowski, M. Ritz, P. Praus, K. Kočí, *J. Phys. Chem. A* **2016**, *120*, 8564–8573. **DOI:**10.1021/acs.jpca.6b07236
42. M. Rutar, N. Rozman, M. Pregelj, C. Bittencourt, R. Cerc Korošec, A. Sever Škapin, A. Mrzel, S. D. Škapin, P. Umek, *Beilstein J. Nanotechnol.* **2015**, *6*, 831–844. **DOI:**10.3762/bjnano.6.86
43. T. Marolt, A. S. Škapin, J. Bernard, P. Živec, M. Gaberšček, *Surf. Coatings Technol.* **2011**, *206*, 1355–1361. **DOI:**10.1016/j.surfcoat.2011.08.053
44. B. Žener, Ž. Medoš, M. Bešter Rogač, R. Cerc Korošec, *ChemistrySelect* **2019**, *4*, 4112–4117. **DOI:**10.1002/slct.201900188
45. S. Yin, Y. Fujishiro, J. Wu, M. Aki, T. Sato, *J. Mater. Process. Technol.* **2003**, *137*, 45–48. **DOI:**10.1016/S0924-0136(02)01065-8
46. D. Yang, H. Liu, Z. Zheng, Y. Yuan, J. C. Zhao, E. R. Waclawik, X. Ke, H. Zhu, *J. Am. Chem. Soc.* **2009**, *131*, 17885–17893. **DOI:**10.1021/ja906774k
47. S. Yin, J. Wu, M. Aki, T. Sato, *Int. J. Inorg. Mater.* **2000**, *2*, 325–331. **DOI:**10.1016/S1466-6049(00)00034-9
48. D. M. Tobaldi, L. Gao, A. F. Gualtieri, A. S. Škapin, A. Tucci, C. Giacobbe, *J. Am. Ceram. Soc.* **2012**, *95*, 1709–1716. **DOI:**10.1111/j.1551-2916.2012.05135.x

Povzetek

Zaradi zmožnosti razgradnje adsorbiranih organskih onesnažil se fotokatalizator TiO_2 v zadnjih desetletjih veliko preučuje za različne okoljske aplikacije. V tem delu predstavljamo z žveplom in dušikom dopirane oz. kodopirane ter s platino modificirane prahove TiO_2, ki smo jih pripravili po koloidnem sol-gel postopku. PXRD meritve kažejo, da zamenjava HCl s H_2SO_4 med sinteznim postopkom zmanjša velikost kristalitov iz ~30 nm na ~20 nm, pri čemer se poveča tudi specifična površina iz ~44 m^2/g na ~80 m^2/g. Opažanja korelirajo z izmerjeno fotokatalitsko aktivnostjo vzorcev in izmerjenim fototokom. Rezultati kažejo, da so lastnosti prahov (specifična površina, velikost kristalitov, obnašanje fototoka) odvisne ne le od vrste uporabljene kisline, temveč tudi od njene količine in uporabljenega dopanta. Dopiranje z žveplom, kodopiranje z žveplom in dušikom in modifikacija prahov TiO_2 s platino povečajo fotokatalitsko aktivnost tudi do šestkrat.